Biosensors and Bioelectronics 146 (2019) 111754

Contents lists available at ScienceDirect

Biosensors and Bioelectronics

journal homepage: http://www.elsevier.com/locate/bios

Magnetic quantum dot based lateral flow assay biosensor for multiplex and sensitive detection of protein toxins in food samples

Chongwen Wang [a,b,d,1], Rui Xiao [b,d,1], Shu Wang [a,e,1], Xingsheng Yang [a], Zikun Bai [b], Xinying Li [c], Zhen Rong [b,d,*], Beifen Shen [c,**], Shengqi Wang [a,b,d,***]

[a] College of Life Sciences, Anhui Agricultural University, Hefei, 230036, PR China
[b] Beijing Institute of Radiation Medicine, Beijing, 100850, PR China
[c] Institute of Basic Medical Sciences, Beijing, 100850, PR China
[d] Beijing Key Laboratory of New Molecular Diagnosis Technologies for Infectious Diseases, Beijing, 100850, PR China
[e] Hefei Institute of Physical Science, Chinese Academy of Sciences, Hefei, PR China

ARTICLE INFO

Keywords:
Magnetic-quantum dot nanoparticles
Fluorescent lateral flow immunoassay
Botulinum neurotoxin type A
Staphylococcal enterotoxin
Simultaneous detection

ABSTRACT

Protein toxins, such as botulinum neurotoxin type A (BoNT/A) and staphylococcal enterotoxin B (SEB), easily pollute food and water and are ultra-toxic to humans and animals, thus requiring a sensitive on-site detection method. In this study, we reported a novel lateral flow assay (LFA) strip on the basis of magnetic quantum dot nanoparticles (MagQD NPs) for sensitive and multiplex protein toxin detection in food samples. A new type of MagQD NP was prepared by fixing the dense carboxylated QDs on the surface of polyethyleneimine-modified Fe_3O_4 magnetic NPs (MNPs) and applied in LFA with the following functions: capture and enrich target toxins from sample solutions and serve as advanced fluorescent labels for the quantitative determination of targets on the strip. Through this strategy, the assay realized quantified BoNT/A and SEB detection in 30 min with the limits of detection of 2.52 and 2.86 pg/mL, respectively. The selectivity and the ability of quantitative analysis of the method were validated in real food samples, including milk and juice. This MagQD-LFA biosensor showed considerable potential as a point-of-care testing tool for the sensitive detection of trace toxins.

1. Introduction

Common protein toxins, which mainly include bacterial toxins such as cholera toxin, botulinum neurotoxins (BoNTs), staphylococcal enterotoxins (SEs), shiga toxin, and phytotoxin ricin, are associated with a number of serious foodborne diseases and huge economic damages (Alam et al., 2012; Duracova et al., 2018; Li et al., 2019). These biotoxins can easy and seriously harm humans' and animals' health by polluting water and food. For example, SEB is a heat-stable enterotoxin that is produced by *Staphylococcus aureus* that is often involved in food poisoning outbreaks (Wang et al., 2016b). Given their extreme toxicity and convenient mass production, some protein toxins are also considered as potential biological weapons for warfare (Zhu et al., 2014). For instance, botulinum neurotoxin type A (BoNT/A) is one of the most powerful toxins known to man and classified as category A biological weapon by the Biological Weapons Convention (Wichert et al., 2019). Given the effectivity of these toxins tin ultralow doses (generally lower than 1 ng/mL), the detection method must be highly sensitive and specific to identify them from complex samples.

Several mature diagnostic technologies, such as live-mouse bioassay, mass spectrometry (MS), high-performance liquid chromatography (HPLC), enzyme-linked immunosorbent assay (ELISA), and various antibody-based methods, have been developed and successfully applied in laboratory tests for protein toxins to date (Duriez et al., 2016; Gehring et al., 2017; Koh et al., 2015; Li et al., 2018; Reverte et al., 2016). All these methods are valuable for the qualitative analyses of toxins, but they have one or more limitations. Mouse bioassay is sufficiently sensitive (with the detection limit of approximately 10 pg/mL) but complex, time-consuming (requires 3–4 days), and ethically questionable (Simon et al., 2015). HPLC and MS analyses require skilled personnel

* Corresponding author.Beijing Institute of Radiation Medicine, Beijing, 100850, PR China.
** Corresponding author.
*** Corresponding author.Beijing Institute of Radiation Medicine, Beijing, 100850, PR China.
E-mail addresses: rongzhen0525@sina.com (Z. Rong), shenbf@mx.cei.gov.cn (B. Shen), sqwang@bmi.ac.cn (S. Wang).
[1] These authors contributed equally to this work.

https://doi.org/10.1016/j.bios.2019.111754
Received 17 July 2019; Received in revised form 20 September 2019; Accepted 30 September 2019
Available online 3 October 2019

and bulky sophisticated instrumentation, thereby limiting their applications in point-of-care testing (POCT) (Li et al., 2017; Rajoria et al., 2017). ELISA and some biosensors can be applied in field detection but generally need a multistep detection process and still lack of multiplex detection ability (Gehring et al., 2017; Hwang et al., 2016). Thus, a sensitive, specific, and simple POCT method for protein toxin detection is urgently needed.

Given its distinct advantages of rapidity, low cost, simple operation, and robustness in applications, lateral flow immunoassay (LFA) strip as a popular POCT technique has been widely applied in various bioanalysis fields (Bahadır and Sezgintürk, 2016; Banerjee and Jaiswal, 2018; Kong et al., 2017; Li and Macdonald, 2016). However, low sensitivity and the lack of quantification ability are the major weaknesses of LFA on the basis of the colorimetric signal readouts (Rong et al., 2019). LFA strips utilizing quantum dot (QD) as label have been developed to improve the sensitivity and quantitative ability (Wang et al., 2017a). Considering its advanced optical properties, the QD-based LFA systems have been successfully used in the quantitative detection of cardiac biomarkers, cancer biomarkers, viruses, and bacteria (Xiao et al., 2019; You et al., 2019). However, for protein toxin detection, two major difficulties must be overcome in using QD-based LFA strip. First, the sensitivity of conventional QD-based LFA strip can not satisfy the requirement for protein toxin detection of quite low concentration. Second, the large amounts of impurities and interferents in real food samples may influence the accuracy of LFA strip for target toxin detection, thereby yielding false results or defects. Magnetic nanomaterials are stable in complex samples and can be easily manipulated to separate and enrich targets by using an external magnetic field, which strongly facilitate the application fields of biosensors (Cheng et al., 2017; Ha et al., 2018; Vermesh et al., 2018). Several previously published studies showed that the combination of magnetic composites, such as Fe_3O_4, Fe_3O_4@Ag, Fe_3O_4–Pt, and Fe_3O_4-QDs, and LFA strip can further improve the sensitivity of LFA biosensors and are extremely suitable for complex sample detection (Duan et al., 2015; Guo et al., 2019; Hu et al., 2019; Kim et al., 2017; Wang et al., 2019). Inspired by these findings, a novel magnetic QD nanoparticle (MagQD NP)-based LFA strip was proposed in this work for the highly sensitive and multiplex detection of two protein toxins (i.e., BoNT and SEB) in food samples. The designed MagQD NP was composed of three parts, as follows: a 160 nm Fe_3O_4 particle that serves as superparamagnetic core, an ultrathin PEI shell that acts as electropositive linker, and dense carboxylated QDs that serve as satellites in providing sufficient fluorescence intensity and as sites for antibody modification. Two immuno-MagQD NPs were prepared by conjugating with BoNT/A and SEB antibodies, respectively, and served as magnetic enrichment tool and enhanced fluorescent probes in the LFA platform. The fluorescence intensities of immuno-MagQDs trapped on the two test lines can be easily read and used for quantitative BoNT/A and SEB detection. Under optimal conditions, the developed MagQD-LFA strip can simultaneously detect BoNT/A and SEB with the limits of detection (LODs) of 2.52 and 2.86 pg/mL, respectively. The analytical performance of the MagQD-LFA strip in terms of selectivity and accuracy was evaluated through testing target toxin-spiked milk and juice. To the best of our knowledge, this work is the first report to introduce MagQD NPs and LFA strip combined system for quantitative and multiplex protein toxin detection.

2. Experimental section

2.1. Materials and reagents

N-(3-dimethyaminopropy)-N′-ethylcarbodiimide hydrochloride (EDC), N-hydroxysulfosuccinimide sodium salt (sulfo-NHS), bovine serum albumin (BSA), 2-(N-morpholino)ethanesulfonic (MES), fetal bovine serum (FBS), and polyvinylpyrrolidone (PVP, MW of 40 kDa) were purchased from Sigma-Aldrich (USA). Diethylene glycol (DEG), ethylene glycol (EG), $FeCl_3{\cdot}6H_2O$, and NaOAc were purchased from Sinopharm Chemical Reagent Co., Ltd. (Shanghai, China). Carboxyl-functionalized CdSe/ZnS QDs (catalog no. CdSe-MPA-625) were purchased from Mesolight Inc (Suzhou, China). Recombinant BoNT/A and SEB proteins, which is a pair of mouse anti-BoNT/A monoclonal antibody, and mouse anti-SEB monoclonal antibody (capture antibody) were acquired from the Academy of Military Medical Sciences (Beijing, China). Mouse anti-SEB monoclonal antibody, which was used as detection antibody (catalog no. S222), was obtained from Santa Cruz Biotechnology (USA). Goat anti-mouse IgG was purchased from Sangon Biotech Co., Ltd. (Shanghai, China). Nitrocellulose membrane (UniSart CN95) with 15 μm pore size was obtained from Sartorius (Spain). The sample loading pad, conjugate pad, absorbent pad, and plastic backing card were purchased from Jieyi Biotechnology Co., Ltd. (Shanghai, China).

2.2. MagQD preparation

The high-performance MagQDs with a core-satellite nanostructure were prepared, as illustrated in Scheme 1a. First, monodispersed Fe_3O_4 MNPs (160 nm) were prepared according to a modified solvothermal reaction, which involves the reduction of $FeCl_3$ with EG and DEG simultaneous reaction by using NaOAc as alkali source and PVP as stabilizer (Wang et al. 2015c, 2016a). Second, the surface self-assembled PEI coating of the magnetic cores was achieved by dispersing 0.1 g Fe_3O_4 MNPs in the PEI aqueous solution (3 mg/mL) under sonication for 30 min (Wang et al., 2015a). After washing three times with deionized water, Fe_3O_4@PEI MNPs were added into sufficient carboxyl-functionalized CdSe/ZnS QD solution and sonicated for 30 min. The process was repeated two times to ensure the full absorption of QDs on the Fe_3O_4@PEI surface. Finally, the Fe_3O_4@PEI-QDs were magnetically separated and acted as MagQDs.

2.3. Immuno-MagQD preparation

Immuno-MagQDs were prepared by conjugating BoNT/A or SEB capture antibody onto the MagQD surface via carbodiimide chemistry. In brief, 2 mg MagQDs was resuspended in 1 mL of MES buffer (100 mM, pH of 6). Then, 100 μL of EDC (10 mM) and 20 μL of sulfo-NHS (100 mM) were added. The mixture was vigorously sonicated for 20 min. Then, excess activators (EDC/sulfo-NHS) were removed from the activated MagQDs through magnetic separation and resuspended in 500 μL of PBS solution (10 mM, pH of 7.4). Then, 15 μg antibody was added, and the mixture was incubated for 2 h at room temperature under shaking at 800 rpm. The unreacted carboxyl groups on the MagQD surface were blocked with 3% BSA for another 1 h. Finally, the antibody-modified MagQDs were magnetically separated, washed two times with PBS (10 mM, pH of 7.4), and resuspended with 300 μL of storage solution (PBS solution containing 0.1% BSA) for follow-up test.

2.4. Multiplex LFA strip preparation for toxin detection

The two test lines and one control line of the NC membrane were separately coated by spraying 1 mg/mL of BoNT/A and SEB monoclonal antibody and 0.8 mg/mL of polyclonal goat anti-mouse IgG to detect the two target toxins. Each antibody was sprayed onto the NC membrane with a dispense rate of 0.1 μL/mm via a spraying platform (Biodot xyz5050). The as-prepared NC membrane was dried in a constant temperature oven at 37 °C for 2 h. Subsequently, the sample pad, conjugate pad, NC membrane, and absorbent pad were assembled onto a plastic backing card. Then, the obtained LFA strips were cut into individual 3 mm wide strips for future use.

2.5. BoNT/A and SEB detection in sample solution via MagQD-based LFA strip

In a typical experiment, 1 mL of toxin sample solution (distilled

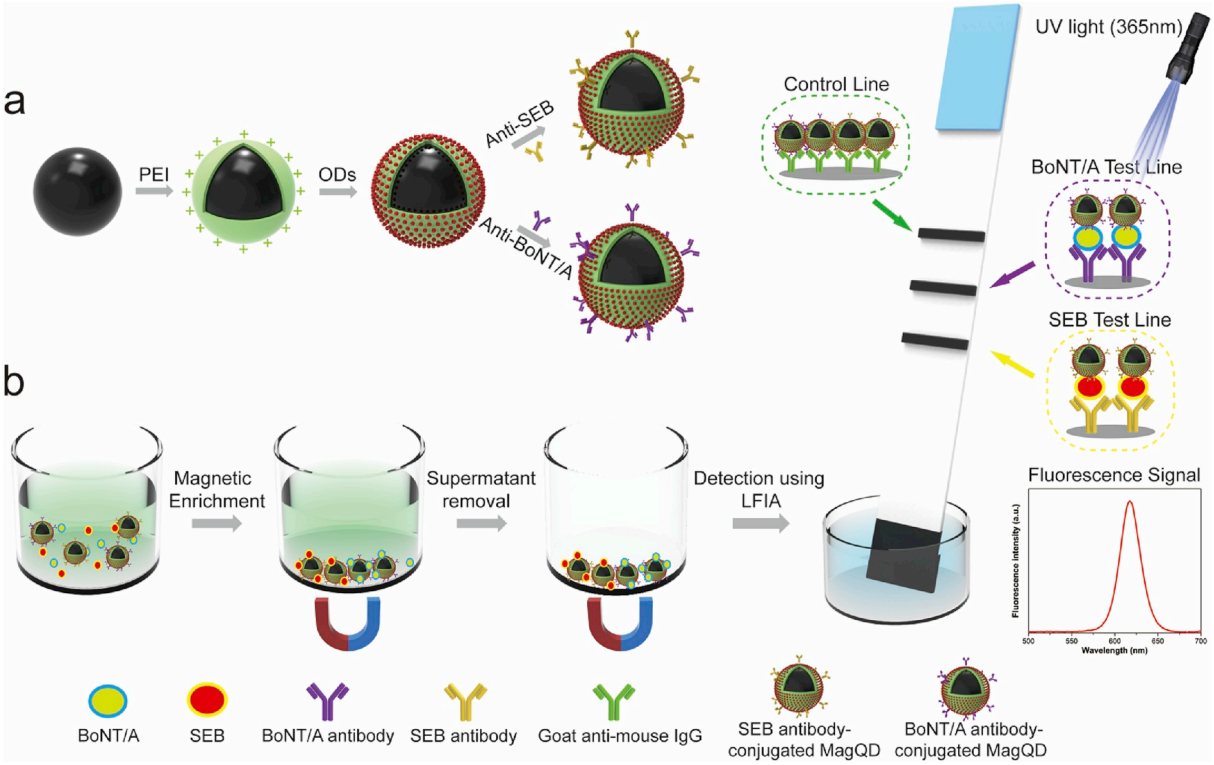

Scheme 1. (a) Scheme of antibody-modified MagQD NP preparation and (b) mechanism of MagQD-based LFA strip for simultaneous and sensitive detection of two protein toxins.

water, milk, or juice) of various concentrations (0–100 ng/mL) was prepared in an Eppendorf (EP) tube. Then, 4 μL of immuno-MagQDs was added in the sample solution, and the EP tube was vigorously shaken for 20 min (800 rpm, 30 °C). Afterward, the immuno-MagQD-toxin complexes were magnetically separated, and the supernatant was discarded. The precipitate was resuspended in 70 μL of running buffer (containing 10 mM PBS, 1% Tween 20, 1% FBS, and 1% BSA). Finally, the LFA strip was inserted vertically into the EP tube for 10 min, and then the fluorescence signal on the test line was recorded using a fluorescent reader (365 nm excitation).

2.6. Instruments

The transmission electron microscopy (TEM) images of QDs, Fe_3O_4 MNPs, and MagQDs were obtained using a Philips Tecnai G2 F20 microscope at an accelerating voltage of 200 kV. The test areas of the LFA strip were examined by scanning electron microscopy (SEM) with a JEOL JSM-7001F microscope. The magnetic property of MagQD NPs was measured using a superconducting quantum interference device magnetometer (MPMSXL-7). The zeta potentials of the synthesized NPs were characterized using Nano-ZS90 Zeta Sizer. The emission spectra of MagQD-based LFA strip were recorded by using a Suzhou Hemai fluorescent strip reader (FIC-S1).

3. Results and discussion

3.1. Strategy for MagQD-based LFA strip

For rapid and sensitive protein toxin detection in food samples, a novel LFA strip biosensor was proposed by using MagQD NPs as replacement for the colloidal Au NPs or QDs NPs, which are used in common LFA strip. The MagQD NPs were fabricated by fixing the dense carboxylated QDs on Fe_3O_4@PEI MNP surface. Given the large amount of QDs on one magnetic particle, the MagQD NPs can generate enough fluorescence signal for ultrasensitive test. The magnetic property of the Fe_3O_4 core enables the MagQD NPs to concentrate the target toxin in the complex solution actively, which can further improve detection sensitivity. Thus, the MagQD NPs combine the advantages of two-component materials and play three roles in the LFA system, that is, capturing, separating, and visualizing target toxin. The proposed MagQD-LFA strip facilitates an indirect detection, and the specific fluorescence signal is produced by the MagQD NPs. Thus, the sensitivity and reliability of the assay highly depend on the performance of MagQD NPs. The size of MagQD NPs was optimized in this study, and the MagQD NPs with 160 nm Fe_3O_4 core was chosed to achieve fast separation and highly sensitive detection of target toxins on the LFA strip. The detailed experimental results were provided in support information S1, and Fig. S1.

Scheme 1b demonstrates the experimental principle of the MagQD-based LFA strip for the two target toxins on the basis of the combination of MagQD NPs and LFA strip. The LFA strip was composed of five components, that is, a sample pad, a NC membrane with plastic backing card, two test lines for the two target toxins, a control line, and an absorbent pad. The BoNT/A detection antibody, SEB detection antibody, and goat anti-mouse IgG antibody were simultaneously dispensed onto the NC membrane to build the two test lines and control line. The assay process can be achieved via three simple steps. First, the antibody-conjugated MagQD NPs were mixed and incubated with the sample solution containing the target toxins under shaking condition. During this process, the target toxins were captured by the MagQD NPs. Afterward, the formed MagQD NP–toxin complexes were easily separated under external magnet and resuspended in the running buffer. In the second step, the running buffer containing MagQD NPs–toxin complexes were loaded onto the sample pad, and then the solution will migrate toward the absorption pad through capillary force. During this process, the MagQD NP–toxin complexes were captured by the antitoxin antibodies on the test zones, thereby forming capture antibody–target–detection antibody sandwich immune complexes. Excess

MagQD NPs continued to migrate and were captured by the goat anti-mouse antibody on the control line of strip. The running buffer was completely drained in 10 min. Finally, the fluorescence intensities of the test lines were measured for highly sensitive and quantitative target toxin detection.

3.2. Characterization of MagQD NP properties

We adopt a self-assembly strategy by coating the Fe_3O_4 MNPs with small QDs through electrostatic interaction. First, 160 nm Fe_3O_4 superparamagnetic NPs were intensely interacted with PEI solution under sonication to form Fe_3O_4@PEI MNPs (Pang et al. 2016). Second, MagQD NPs were fabricated by adsorbing carboxylated CdSe/ZnS QDs (15 nm) on the surface of Fe_3O_4@PEI MNPs densely and firmly via the strong positive electricity of PEI. High-resolution TEM was performed to verify the morphology of the prepared MagQD NPs. Fig. 1a, b, and c show the TEM images of QDs, Fe_3O_4@PEI MNPs, and MagQD NPs, respectively. The distribution of CdSe/ZnS QDs on the Fe_3O_4@PEI surface was uniform. The high amount of carboxyl-functionalized QDs that was immobilized on the Fe_3O_4@PEI MNPs not only produced a significantly enhanced fluorescence signal but also provided large surface sites for antibody modification. Fig. 1d displays the EDS elemental mapping result of MagQD NPs. Dense Cd element (blue) was located on the Fe element (red) surface, which was consistent with the Fe_3O_4–CdSe/ZnS core–satellite nanostructure. The zeta potentials of the carboxyl-functionalized QDs, Fe_3O_4, and Fe_3O_4@PEI MNPs were −6.9, −27.2, and +40.8 mV, respectively (Fig. 1e). The strong positive surface charge of the Fe_3O_4@PEI MNPs was effective for electrostatic adsorption (Wang et al., 2015b). After the adsorption of carboxylated QDs on the Fe_3O_4@PEI MNPs, the zeta potential of the formed MagQD NPs became negative again (−3.7 mV) due to the numerous negatively charged QDs on the surface.

Next, we investigated the fluorescence intensity of MagQD NPs. The fluorescence spectra of CdSe/ZnS QDs, Fe_3O_4, and MagQD NPs are displayed in Fig. 1f. The MagQD NPs showed significant fluorescence signals that were as strong as that of CdSe/ZnS QDs at 615 nm by excitation with a single ultraviolet (UV) light (365 nm). The fluorescence intensity of the MagQD NPs was relatively stable and remained unchanged at 4 °C in ethanol for 3 months (Fig. S2). The magnetic properties of the MagQD NPs were also investigated and are displayed in Fig. 1g. The saturation magnetization (MS) value of 160 nm Fe_3O_4 MNPs was 82.2 emu/g. Although the MS values gradually decreased with PEI coating (72.4 emu/g) and QD adsorption (61.5 emu/g), the superior magnetite content (ca. 74.8 wt%) can also guarantee the complete separation of MagQD NPs from the sample solution quickly (within 1 min) under an external magnet.

3.3. MagQD-based LFA strip optimization

The excellent fluorescent and magnetic properties enable the MagQD NPs as the high-performance fluorescent nanotags for LFA strip detection. Immuno-MagQD NPs can simply be prepared by labeling antitoxin antibodies to the surface carboxyl groups of the MagQD NPs directly through amido linkages. The inner hemisphere of carboxylated QDs was direct contact with PEI shell, thus the NH_2 groups of PEI and COOH groups of QDs could form amide bonds via carbodiimide activation. This self-binding of MagQDs can further stabilize the whole nanostructure. In this study, the high-quality immuno-MagQD NPs were prepared by using excessive amount of antibody. The maximum load capacity of antibody on the surface of MagQD NPs was investigated by incubating 5, 10, 15, and 20 μg of SEB antibody with 1 mL of MagQD NPs (1 mg/mL), respectively. Then, the antibody-conjugated MagQD NPs were blocked with 3% BSA (w/v), and used for LFA strip detection. Positive sample (SEB, 10 ng/mL) and negative sample solutions were tested by the assay to investigate the signal-to-noise ratio (SNR) of test line. As shown in Fig. S3a, the increasing antibody amount from 5 μg to 15 μg not only enhances the signal intensity by improving the efficiency of immune complex formation but also decreases noise intensity by preventing the aggregation of MagQD NPs. The fluorescence signal of 15 μg antibody modified MagQD NPs was strong enough and very stable for LFA detection, indicating that the surface of the MagQD NPs has been saturated with antibody. The dynamic light scattering (DLS) results in Fig. S3b showed that the average diameter of MagQD NPs increased from 198 nm to 210 nm after antibody modification. UV absorption at

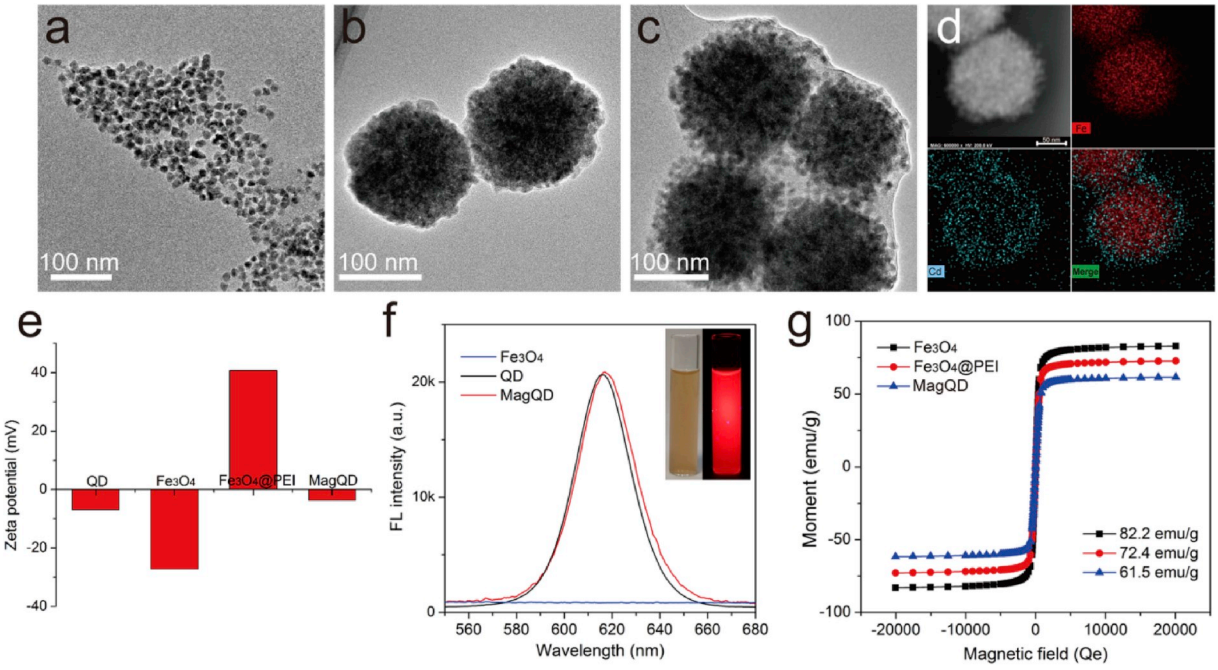

Fig. 1. Characterization of the synthesized MagQD. TEM images of (a) CdSe@ZnS QDs, (b) Fe_3O_4 MNPs, and (c) MagQDs. (d) Elemental mapping images of single MagQD. The zeta potential (e), fluorescence emission spectra (f), and magnetic hysteresis curves (g) of the prepared MagQDs. The inset in (f) shows the photographs of MagQD solution under visible (left) and ultraviolet light (right).

280 nm of the supernatants of immuno-MagQD NPs significantly decreased after antibody conjugation (Fig. S3c). All these results showed the successful conjugation of antibody on the surface of immuno-MagQD NPs.

We first used anti-SEB antibody-modified MagQD NPs to verify the performance of the proposed MagQD-based LFA strip. The types of running buffer and NC membrane (CN95) were adopted from our previously reported magnetic SERS strip system, which has been carefully optimized and are suitable for Fe_3O_4 particle-based LFA strip (Wang et al., 2019). The detection process was executed as follows: capture, magnetic enrichment, and reaction on the LFA strip. The aggregation of MagQDs on the test line showed an evident orange-yellow band when 1 mL of SEB distilled water sample (10 ng/mL) was applied (Fig. 2a, i). By contrast, no visible band was observed at the test zone in the absence of SEB (Fig. 2b, i). When induced by UV light (365 nm), bright red fluorescence appeared on the test line of the positive group (Fig. 2a, ii), whereas no fluorescence signal can be observed at the negative one (Fig. 2b, ii). The SEM images of the test lines were used to verify that the red fluorescence was from MagQDs. As shown in Fig. 2a iii and 2b iii, a large number of MagODs were observed in the test line of the positive group, and none was observed in the negative group, respectively. All these findings indicated that the MagQD-SEB complexes were captured on the test line of NC membrane through forming antibody-antigen-antibody sandwich-like structure. The fluorescence intensity was proportional to the amount of sandwich-like immunocomplex accumulated on the test line (Huang et al., 2019). All the tested groups had a visible orange-yellow band on the control line, which indicated that the immuno-MagQD NPs had recognition activity. Thus, it can be captured by the anti-mouse IgG. The bright control line proved that the LFA strip was working correctly (Zhang et al., 2018).

For the further optimization of the detection capability of the MagQD-based LFA strip, the effects of antibody concentration loaded on the test line and immuno-MagQD incubation time were investigated. Fig. 2c reveals that 1 mg/mL of detection antibody that was loaded on the test line generated the highest SNR of the fluorescence intensity. As shown in Fig. 2d, with the increase in incubation time in the magnetic enrichment process, the fluorescence intensity of the test line increased, and the signal value reached saturation in 20 min. Thus, the optimal parameters were determined and used in the MagQD-based LFA strip system.

It should be noted that the antibody conjugated-MagQD NPs are unstable at a higher temperature. To ensure the stability of immuno-MagQD NPs, the freshly prepared immuno-MagQD NPs were divided into small pieces, prepared by vacuum freeze-drying and stored at 4 °C (Fig. S4a). As shown in Fig. S4b, the fluorescence intensity and average hydrodynamic diameter of immuno-MagQD NPs remained unchanged for 90 days in water, which indicated that the freeze-dried MagQD NPs have high stability. The long-term stability of MagQD-LFA strip was tested as shown in Fig. S4c, the fluorescence intensity of the test lines was stable after 90 days storage. All these results indicate the good stability of our proposed MagQD-LFA strip.

3.4. Multiplex detection capability of MagQD-based LFA strip

To test the multiplex detection capability of our proposed MagQD-based LFA strip, we simultaneously detected two common protein toxins, that is, BoNT/A and SEB, by using MagQD-based LFA strip biosensor in the same test. As illustrated in Scheme 1b, BoNT/A and SEB capture antibodies were modified on the MagQD NPs, and the corresponding detection antibodies were separately spotted on the strip with 3 mm interval for the combined detection of the two target toxins. First, a series of BoNT/A and SEB solutions was detected following optimal experimental conditions via the LFA strip. As displayed in Fig. 3a, the digital photographic and fluorescence images demonstrated the corresponding color changes of the test lines for different BoNT/A and SEB concentrations, and no cross reactions were observed between the two target toxins in the LFA strip. The fluorescence spectra and detailed intensity values can be easily determined by a commercial fluorescent reader, as shown in Fig. 3b and c, respectively. Thus, the simultaneous and quantitative analyses of BoNT/A and SEB on the LFA strip is possible by reading the fluorescence intensity of the two test lines.

Subsequently, we assessed the test sensitivity and linearity range of MagQD-based LFA strip for the simultaneous detection of the two target toxins. Fig. 4a and b shows the digital photographic images and the fluorescence images of two separate test lines for the two toxin groups (from 100 ng/mL to 0 ng/mL). The visible yellow color and red fluorescence of MagQD NPs were found on the test lines at high concentration, and the intensity gradually decreased with the decrease in toxin concentration. The visible yellow test lines for BoNT/A and SEB can be observed with the naked eye at a concentration of 1 ng/mL (Fig. 4a). The

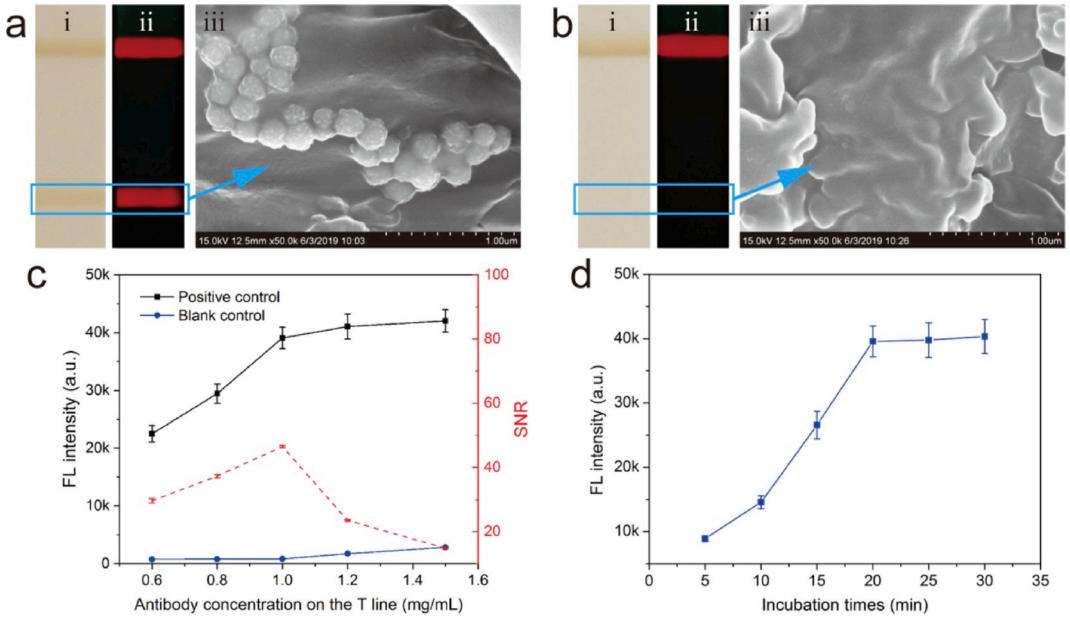

Fig. 2. Photographs (i), fluorescence images (ii), and SEM images (iii) of MagQD-based LFA strip test line with (a) and without (b) a target toxin. Effects of experimental conditions on the test line intensity: (c) detection antibody concentration and (d) MagQD incubation times.

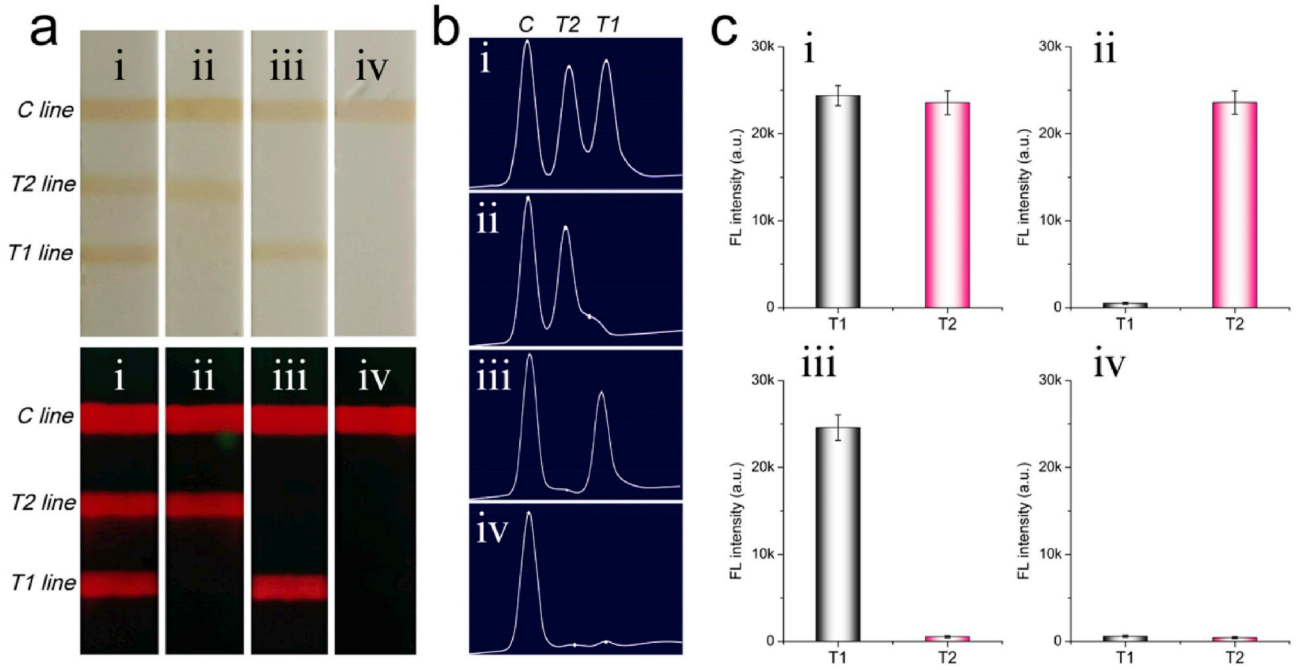

Fig. 3. (a) Photographs, (b) corresponding fluorescence signal, and (c) fluorescence intensity of MagQD-based LFA strip with (i) 10 ng SEB and 10 ng BoNT/A, (ii) 0 ng SEB and 10 ng BoNT/A, (iii) 10 ng SEB and 0 ng BoNT/A, and (iv) 0 ng SEB and 0 ng BoNT/A.

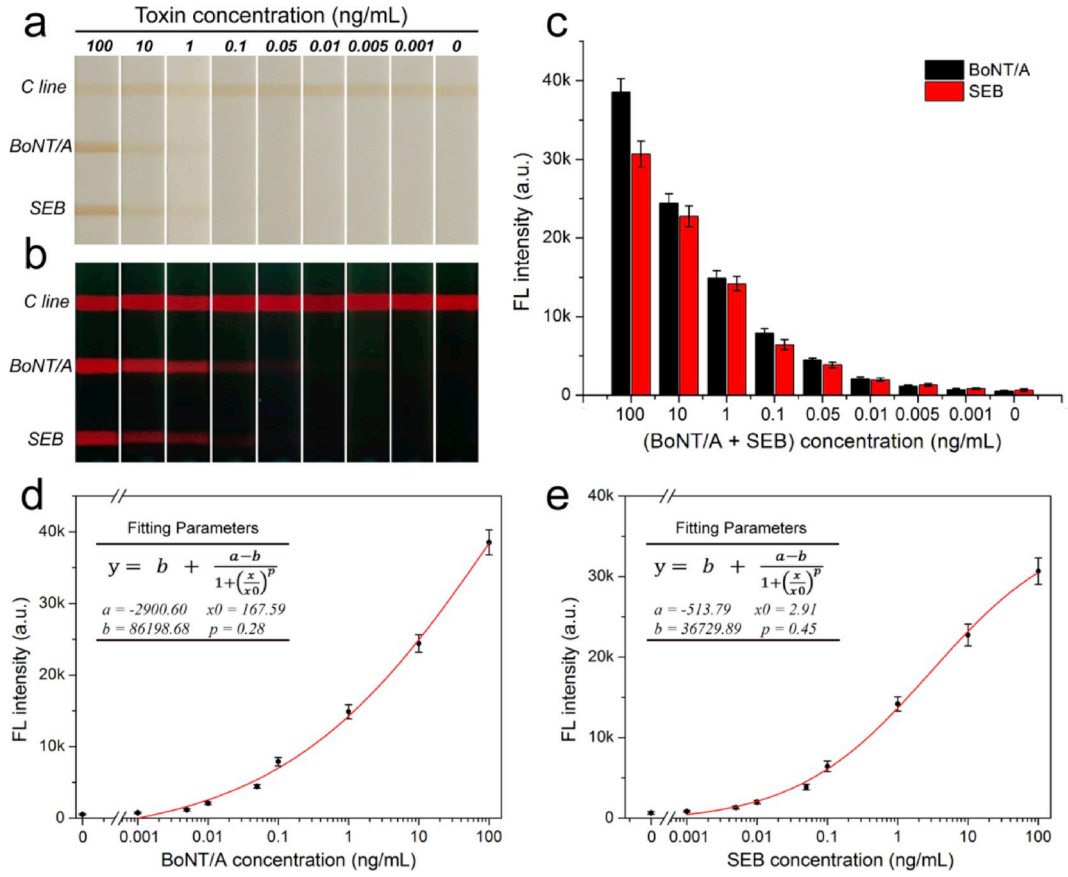

Fig. 4. (a) Photographs, (b) fluorescence pictures, and (c) corresponding test line intensities for different BoNT/A and SEB concentrations in distilled water ranging from 0 ng/mL to 100 ng/mL. Corresponding calibration curves for (d) BoNT/A and (e) SEB. Insets showed the four-parameter sigmoid function for the fitting curves. Error bars represented the standard deviations that were calculated from the five separate experiments.

visual detection limit was relatively high and cannot meet the practical requirement for toxin detection. However, the fluorescence signal results revealed that the visualization limit for the two target toxins was as low as 10 pg/mL (Fig. 4b). For the fluorescence detection mode, the quantitative analyses of BoNT/A and SEB were feasible by measuring the fluorescence intensity of the MagQD NPs on the test zones. The corresponding fluorescence numerical results of Fig. 4b that were readouts from the commercial fluorescent reader are shown in Fig. 4c. The error bars indicated the standard deviations from the five separate tests. According to the fluorescence data, the corresponding calibration curves for BoNT/A and SEB were constructed, as shown in Fig. 4d and e, respectively. The plot for toxins exhibited logarithmic relationship with small standard deviations over a wide detection range (1 pg/mL–100 ng/mL). The four-parameter sigmoid function for the fitting curves are shown in the insets of Fig. 4d and e. The LODs of the two toxins via MagQD-based LFA strip were determined according to the IUPAC guidelines, as follows: $LOD = y_{blank} + 3 \times SD_{blank}$, where y_{blank} and SD_{blank} are the average fluorescence intensity and standard deviation of the blank control, respectively (Hu et al., 2017; Wang et al., 2017b). According to the formula above, the LODs were 2.52 pg/mL for BoNT/A and 2.86 pg/mL for SEB. The detection sensitivity of the fluorescent LFA strip on the basis of MagQD NPs was significantly improved by approximately 396-fold for BoNT/A and 349-fold for SEB compared with those of colorimetric results.

To compare the sensitivity of the MagQD-based LFA strip with those of traditional immunoanalytical approaches further, we conducted a set of ELISA analysis for BoNT/A and SEB by using the same immunoreagents. Fig. S5 reveals that the developed MagQD-based LFA strips were approximately five times more sensitive than the ELISA method and had a wider dynamic range. The MagQD-based LFA strip enabled reproducible and sensitive toxin detection within 30 min, which included a 20 min magnetic enrichment time. Meanwhile, the commonly used ELISA method required several hours of assay time (ca. 3–5 h) (de la Rica and Stevens, 2012; Gehring et al., 2017). The specificity of the MagQD-based LFA strip was investigated using other toxins as interferents, which are commonly found in food, including aflatoxin B_1, ricin, and staphylococcal enterotoxin A (Li et al., 2017). As shown in Figs. S6 and 100 ng/mL interferents and blank control group did not exhibit fluorescence signal, whereas low-concentration BoNT/A (1 ng/mL) or SEB (1 ng/mL) showed a distinct signal. These results indicated that the MagQD-based LFA strip had good selectivity for target BoNT/A and SEB detection.

3.5. Target toxin detection in real food samples

The developed MagQD-based LFA strip on the basis of the antibody-modified magnetic-QDs core–satellite NPs was used for the efficient capture of the target toxins to separate them from the solution. Magnetic particles have good stability in complex solutions (Peng et al., 2018; Razo et al., 2018). Thus, the MagQD-based LFA strip has potential for direct application in real food samples. Given that the most common way of intoxication is through food products, the analytical performance of the assay for real samples is one of our focuses. To test the anti-interference ability in food samples, we used MagQD-LFA system to measure the two target toxins in milk and grape juice. Different BoNT/A and SEB concentrations (0.1–10 ng/mL) were spiked into the milk and grape juice, respectively. The juice sample was pretreated using a 0.2 μm syringe filter to remove pulp residue, while the milk sample did not need sample pretreatment. Then, the detection process was carried out according to the developed protocol. Fig. 5 reveals that the milk and grape juice groups at a concentration of 10 ng/mL also produced strong fluorescence signals, and their intensity only suffered minor weakness. The results indicated that the assay can work well in complex food samples. Six different batches of MagQD-LFA strips were used to test the repeatability of the assay in the SEB-spiked milk (10 ng/mL). As shown in Fig. S7, MagQD-LFA system had good repeatability and high

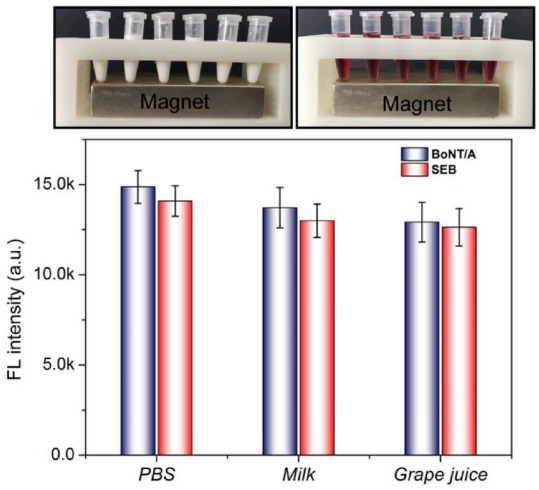

Fig. 5. Detection results of real food samples (milk and grape juice) with BoNT/A and SEB (10 ng/mL). Error bars are the standard deviation of three repetitive experiments.

reliability in real samples. The relative standard deviation (RSD) value of the fluorescence intensity was 3.86%. To further investigate the stability of MagQD-LFA strip, a set of control experiment was performed at three different temperatures: 4 °C, 25 °C (room temperature), and 37 °C according to the developed protocol. Three independent tests were conducted to measure SEB samples at concentrations of 10, 0.1, and 0 ng/mL. As shown in Fig. S8, the proposed MagQD-LFA strip has excellent stability and signal repeatability under the different temperature condition (4 °C–37 °C).

Then, recovery tests were conducted in food samples to evaluate the accuracy and precision of the MagQD-based LFA strip. As summarized in Table 1, the average recovery values of this method were 86.4%–98.0% and 78.8%–93.1% for milk and juice samples, respectively, with the RSD ranging from 3.0% to 10.3%. The low RSD values also indicated the good repeatability of our method. Combined with its easy-to-use format, the proposed MagQD-based LFA strip showed strong potential for multiplex and sensitive toxin detection in real food samples. The MagQD-based LFA system can be directly applied for the detection of the other protein toxins by changing the specific detection antibodies. With the help of a portable fluorescent LFIA reader, the MagQD-based LFA strip had considerable potential and prospect for sensitive toxin detection in complex food matrixes.

4. Conclusions

We reported a simple, sensitive, and multichannel LFA biosensor for BoNT/A and SEB detection by using magnetic QDs as active fluorescent probe. MagQD NPs were prepared using PEI-mediated adsorption method, which ensured that the nanocomposites possessed monodispersity, excellent magnetic property, and high luminescence. After the optimization of the experimental parameters, the proposed MagQD-based LFA system was an effective tool for the specific capture and magnetic enrichment of target toxins in food samples and fluorescent quantitative analysis of targets on the strip. MagQD-strip is capable of ultrasensitive quantification and simultaneous detection of the two target toxins with wide dynamic range. The LOD values for BoNT/A and SEB were 2.52 and 2.86 pg/mL, respectively. The superior specificity and potential uses of the assay in real food samples were also proven. Further considering the other merits including ease of operation, fast detection time, low cost and good reproducibility, MagQD-based LFA strip has great potential as a POCT tool for toxins actual detection.

Table 1
BoNT/A and SEB detection results in spiked in milk and grape juice.

Sample	Added toxin (ng/mL)		Detected toxin (ng/mL)		Recovery (%)		RSD (%)	
	BoNT/A	SEB	BoNT/A	SEB	BoNT/A	SEB	BoNT/A	SEB
Milk	10	10	8.91 ± 0.46	8.64 ± 0.39	89.1	86.4	3.0	3.7
	1	1	0.92 ± 0.14	0.93 ± 0.18	92.4	93.5	8.4	7.5
	0.1	0.1	0.095	0.098	95.0	98.0	8.2	9.1
Grape juice	10	10	8.16 ± 0.31	7.88 ± 0.71	81.6	78.8	3.5	4.1
	1	1	0.87 ± 0.24	0.83 ± 0.58	87.0	83.0	8.7	10.3
	0.1	0.1	0.091	0.093	91.0	93.1	9.7	8.5

Declaration of competing interest

The authors declare that they have no known competing financial interests or personal relationships that could have appeared to influence the work reported in this paper.

CRediT authorship contribution statement

Chongwen Wang: Conceptualization, Methodology, Writing - original draft. **Rui Xiao:** Methodology, Writing - original draft. **Shu Wang:** Methodology, Writing - original draft. **Xingsheng Yang:** Methodology. **Zikun Bai:** Methodology. **Xinying Li:** Methodology. **Zhen Rong:** Methodology, Writing - review & editing, Supervision. **Beifen Shen:** Writing - review & editing, Supervision. **Shengqi Wang:** Writing - review & editing, Supervision.

Acknowledgements

This study was supported by the National S&T Major Project for Infectious Diseases Control (Grant nos. 2018ZX10712001-010, 2018ZX10101003-001), the National Natural Science Foundation of China (Grant no. 81830101), and the Natural Science Foundation of Anhui Province (Grant no. 1908085QB85).

Appendix A. Supplementary data

Supplementary data to this article can be found online at https://doi.org/10.1016/j.bios.2019.111754.

References

Alam, S.I., Kumar, B., Kamboj, D.V., 2012. Anal. Chem. 84, 10500–10507.
Bahadır, E.B., Sezgintürk, M.K., 2016. Trac. Trends Anal. Chem. 82, 286–306.
Banerjee, R., Jaiswal, A., 2018. Analyst 143, 1970–1996.
Cheng, Z., Choi, N., Wang, R., Lee, S., Moon, K.C., Yoon, S.Y., Chen, L., Choo, J., 2017. ACS Nano 11, 4926–4933.
de la Rica, R., Stevens, M.M., 2012. Nat. Nanotechnol. 7, 821–824.
Duan, D., Fan, K., Zhang, D., Tan, S., Liang, M., Liu, Y., Zhang, J., Zhang, P., Liu, W., Qiu, X., Kobinger, G.P., Fu Gao, G., Yan, X., 2015. Biosens. Bioelectron. 74, 134–141.
Duracova, M., Klimentova, J., Fucikova, A., Dresler, J., 2018. Toxins 10, 99.
Duriez, E., Armengaud, J., Fenaille, F., Ezan, E., 2016. J. Mass Spectrom. 51, 183–199.
Gehring, A.G., Fratamico, P.M., Lee, J., Ruth, L.E., He, X., He, Y., Paoli, G.C., Stanker, L. H., Rubio, F.M., 2017. Food Control 77, 145–149.
Guo, L., Shao, Y., Duan, H., Ma, W., Leng, Y., Huang, X., Xiong, Y., 2019. Anal. Chem. 91, 4727–4734.
Ha, Y., Ko, S., Kim, I., Huang, Y., Mohanty, K., Huh, C., Maynard, J.A., 2018. ACS Appl. Nano Mater. 1, 512–521.
Hu, J., Jiang, Y.Z., Tang, M., Wu, L.L., Xie, H.Y., Zhang, Z.L., Pang, D.W., 2019. Anal. Chem. 91, 1178–1184.
Hu, J., Jiang, Y.Z., Wu, L.L., Wu, Z., Bi, Y., Wong, G., Qiu, X., Chen, J., Pang, D.W., Zhang, Z.L., 2017. Anal. Chem. 89, 13105–13111.
Huang, Z., Peng, J., Han, J., Zhang, G., Huang, Y., Duan, M., Liu, D., Xiong, Y., Xia, S., Lai, W., 2019. Food Chem. 276, 333–341.
Hwang, J., Lee, S., Choo, J., 2016. Nanoscale 8, 11418–11425.
Kim, M.S., Kweon, S.H., Cho, S., An, S.S.A., Kim, M.I., Doh, J., Lee, J., 2017. ACS Appl. Mater. Interfaces 9, 35133–35140.
Koh, C.Y., Schaff, U.Y., Piccini, M.E., Stanker, L.H., Cheng, L.W., Ravichandran, E., Singh, B.R., Sommer, G.J., Singh, A.K., 2015. Anal. Chem. 87, 922–928.
Kong, M., Shin, J.H., Heu, S., Park, J.K., Ryu, S., 2017. Biosens. Bioelectron. 96, 173–177.
Li, J., Macdonald, J., 2016. Biosens. Bioelectron. 83, 177–192.
Li, Q., Lu, Z., Tan, X., Xiao, X., Wang, P., Wu, L., Shao, K., Yin, W., Han, H., 2017. Biosens. Bioelectron. 97, 59–64.
Li, S.J., Sheng, W., Wen, W., Gu, Y., Wang, J.P., Wang, S., 2018. Mikrochim. Acta 185, 238.
Li, X., Wang, J., Yi, C., Jiang, L., Wu, J., Chen, X., Shen, X., Sun, Y., Lei, H., 2019. Sens. Actuators B Chem. 290, 170–179.
Pang, Y., Wang, C., Wang, J., Sun, Z., Xiao, R., Wang, S., 2016. Biosens. Bioelectron. 79, 574–580.
Peng, B., Zhang, X., Aarts, D., Dullens, R.P.A., 2018. Nat. Nanotechnol. 13, 478–482.
Rajoria, S., Kumar, R.B., Gupta, P., Alam, S.I., 2017. Anal. Chem. 89, 4062–4070.
Razo, S.C., Panferov, V.G., Safenkova, I.V., Varitsev, Y.A., Zherdev, A.V., Dzantiev, B.B., 2018. Anal. Chim. Acta 1007, 50–60.
Reverte, L., Prieto-Simon, B., Campas, M., 2016. Anal. Chim. Acta 908, 8–21.
Rong, Z., Wang, Q., Sun, N., Jia, X., Wang, K., Xiao, R., Wang, S., 2019. Anal. Chim. Acta 1055, 140–147.
Simon, S., Fiebig, U., Liu, Y., Tierney, R., Dano, J., Worbs, S., Endermann, T., Nevers, M. C., Volland, H., Sesardic, D., Dorner, M.B., 2015. Toxins 7, 5011–5034.
Vermesh, O., Aalipour, A., Ge, T.J., Saenz, Y., Guo, Y., Alam, I.S., Park, S.-m., Adelson, C. N., Mitsutake, Y., Vilches-Moure, J., Godoy, E., Bachmann, M.H., Ooi, C.C., Lyons, J. K., Mueller, K., Arami, H., Green, A., Solomon, E.I., Wang, S.X., Gambhir, S.S., 2018. Nat. Biomed. Eng. 2, 696–705.
Wang, C., Li, P., Wang, J., Rong, Z., Pang, Y., Xu, J., Dong, P., Xiao, R., Wang, S., 2015. Nanoscale 7, 18694–18707.
Wang, C., Qian, J., An, K., Huang, X., Zhao, L., Liu, Q., Hao, N., Wang, K., 2017. Biosens. Bioelectron. 89, 802–809.
Wang, C., Wang, C., Wang, X., Wang, K., Zhu, Y., Rong, Z., Wang, W., Xiao, R., Wang, S., 2019. Magnetic SERS strip for sensitive and simultaneous detection of respiratory viruses. ACS Appl. Mater. Interfaces 11, 19495–19505.
Wang, C., Wang, J., Li, P., Rong, Z., Jia, X., Ma, Q., Xiao, R., Wang, S., 2016. Nanoscale 8, 19816–19828.
Wang, C., Xu, J., Wang, J., Rong, Z., Li, P., Xiao, R., Wang, S., 2015. J. Mater. Chem. C 3, 8684–8693.
Wang, J., Wu, X., Wang, C., Shao, N., Dong, P., Xiao, R., Wang, S., 2015. ACS Appl. Mater. Interfaces 7, 20919–20929.
Wang, W., Wang, W., Liu, L., Xu, L., Kuang, H., Zhu, J., Xu, C., 2016. ACS Appl. Mater. Interfaces 8, 15591–15597.
Wang, X., Choi, N., Cheng, Z., Ko, J., Chen, L., Choo, J., 2017. Anal. Chem. 89, 1163–1169.
Wichert, W.R.A., Dhummakupt, E.S., Zhang, C., Mach, P.M., Bernhards, R.C., Glaros, T., Manicke, N.E., 2019. Detection of protein toxin simulants from contaminated surfaces by paper spray mass spectrometry. J. Am. Soc. Mass Spectrom. 30, 1406. https://doi.org/10.1007/s13361-019-02141-6.
Xiao, M., Huang, L., Dong, X., Xie, K., Shen, H., Huang, C., Xiao, W., Jin, M., Tang, Y., 2019. Analyst 144, 2594–2603.
You, P.Y., Li, F.C., Liu, M.H., Chan, Y.H., 2019. ACS Appl. Mater. Interfaces 11, 9841–9849.
Zhang, D., Huang, L., Liu, B., Ni, H., Sun, L., Su, E., Chen, H., Gu, Z., Zhao, X., 2018. Biosens. Bioelectron. 106, 204–211.
Zhu, K., Dietrich, R., Didier, A., Doyscher, D., Martlbauer, E., 2014. Toxins 6, 1325–1348.